Applied Energy 88 (2011) 1113–1119

Contents lists available at ScienceDirect

Applied Energy

journal homepage: www.elsevier.com/locate/apenergy

Numerical study on NO_x/CO emissions in the diffusion flames of high-temperature off-gas of steelmaking converter

Sen Li *, Xiaolin Wei, Linxin Yu

Institute of Mechanics, Chinese Academy of Sciences, No.15 Beisihuanxi Road, Beijing 100190, China

ARTICLE INFO

Article history:
Received 24 April 2010
Received in revised form 8 October 2010
Accepted 21 October 2010

Keywords:
Off-gas of steelmaking converter
NO_x
CO
Counterflow diffusion flame

ABSTRACT

The combustion of high-temperature off-gas of steelmaking converter with periodical change of temperature and CO concentration always leads to CO and NO_x over-standard emissions. In the paper, high-temperature off-gas combustion is simulated by adopting counterflow diffusion flame model, and some influencing factors of CO and NO_x emissions are investigated by adopting a detailed chemistry GRI 3.0 mechanism. The emission index of NO_x ($EINO_x$) decreases 1.7–4.6% when air stoichiometric ratio (SR) increase from 0.6 to 1.4, and it dramatically increases with off-gas temperature at a given SR when the off-gas temperature is above 1500 K. High-concentration CO in off-gas can result in high NO_x emissions, and NO_x levels increase dramatically with CO concentration when off-gas temperature is above 1700 K. Both SR and off-gas temperature are important for the increase of CO burnout index (BI_{CO}) when SR is less than 1.0, but BI_{CO} increase about 1% when off-gas temperature increases from 1100 K to 1900 K at SR > 1.0. BI_{CO} increases with CO concentration in off-gas, and the influence of off-gas temperature on BI_{CO} is marginal. BI_{CO} increases with the relative humidity (RH) in air supplied, but it increases about 0.5% when RH is larger than 30%.

1. Introduction

Blown oxygen converter steelmaking has developed for over 50 years, and the process is retaining its predominance as the world's No. 1 steelmaking method by technological innovation [1]. The oxygen steelmaking process is a very complex batch reaction course. Decarburization of molten metal is a basic process of oxygen converter steelmaking, and the process is determined by the development of heat and mass transfer processes in the bath. A characteristic of converter steelmaking production is the formation of a large amount of high-temperature off-gas, and the main compositions are CO and CO_2. Off-gas is a precious valuable fuel containing high-concentration CO, CO concentration and temperature periodically change during blown oxygen steelmaking, CO concentration varies from 0 to 80%, and off-gas temperature can reach 1900 K [2]. Therefore, off-gas of steelmaking converter is an important secondary energy resource for steel enterprises, and it is important for steel enterprises to effectively recover off-gas energy.

In order recover off-gas energy, off-gas of steelmaking converter is often discharged into the cooling stack to be combusted and cooled in practical steelmaking process. The cooling stack is installed above the outlet of converter in which off-gas is combusted. The cooling stack often comprises movable hood and four fixed sections [3]. During steelmaking, the cooling stack is under negative pressure, the movable hood of cooling duct is raised, off-gas is discharged into the cooling stack, a large amount of air is sucked from ambient atmosphere, and then off-gas is combusted by the sucked air. However, the improper mode of air sucked makes CO burnout difficult, and high-temperature off-gas combustion results in NO_x formation. For the diffusion combustion of high-temperature off-gas in the cooling stack, the diffusions of air and off-gas effect the flame temperature, local maximum temperature can reach above 2300 K, where CO_2 may decompose and NO_x is formed at a significant rate. CO emission concentration at the cooling stack outlet can reach above 2000 mg/m^3 which is always over emission standard (300 mg/m^3 in China) [4,5]. CO is a toxic gas which is dangerous to human health, high CO emission results in not only atmospheric pollutant but also fuel loss. NO_x is a known precursor to the formation of ozone and acid rain, and it can react with volatile organic compounds to form photo-chemical smog [6].

At present, the control of pollutant emissions during steelmaking process mainly focus on the dusts [4], and the control of CO and NO_x emissions is not paid sufficient attentions in iron and steel industry. In order understand the diffusion flames of off-gas to improve combustion efficiency and to reduce the gaseous pollutants, the numerical study on NO_x and CO emissions in off-gas counterflow diffusion flame, by adopting counterflow diffusion

* Corresponding author. Tel.: +86 10 82544231.
E-mail address: lisen@imech.ac.cn (S. Li).

0306-2619/$ - see front matter © 2010 Elsevier Ltd. All rights reserved.
doi:10.1016/j.apenergy.2010.10.030

Nomenclature

δ_{mix}	the mixing layer thickness counterflow flame (cm)
D	gas mass diffusion coefficient (cm^2/s)
χ	scalar dissipation rate
α_g	global strain rate (s^{-1})
ρ	the density of the reactant streams (kg/m^3)
L	the duct separation distance (cm)
SR	air stoichiometric ratio
RH	the relative humidity in air (%)
X	the relative axial distance from fuel jet port
T_{max}	the maximum temperature of flame
$EINO_x$	the emission index of NO_x
W_i	the molecular weight and molar production rate of species i
w_i	the molar production rate of species i
BI_{CO}	CO burnout index

flame as a model, the influences of air stoichiometric ratio (SR), the CO concentration in off-gas, off-gas temperature and the relative humidity (RH) of air supplied on CO and NO_x emissions are investigated by adopting a detailed chemistry model using Cantera software code [7,8].

2. Numerical model

The axisymmetric laminar diffusion flame has attracted much attention as a model system with a relatively simple geometry and sharing many properties with flames in practical devices [9]. A counterflow diffusion flame offers a convenient geometry in modeling the detailed processes that occur in diffusion flames [10]. The counterflow geometry is well known, which consists of two concentric, circular nozzles directed towards each other, and this configuration produces an axisymmetric flow field with a stagnation plane between the nozzles, as shown in Fig. 1 [11].

The actual flow field in the counterflow is two-dimensional, and the two-dimensional flow can be reduced to one dimension by some simplifications. The mathematical treatment can be simplified considerably if the description is restricted to the flow properties along the stagnation stream line in Fig. 1. Based on the boundary layer approximation of Prandtl [12] (neglect of diffusion in the direction orthogonal to the stream, in Fig. 1 the y direction), the problem reduces to one spatial coordinate, namely the distant from the stagnation line or point, respectively. In this way, the tangential gradients of temperature and mass fractions, and the velocity component v can be eliminated. Here, there are assumptions: (1) the temperature and mass fractions of all species are functions solely of the coordinate x normal to the flame; (2) the normal velocity u is a function of x only; (3) the tangential velocity v is proportional to the coordinate tangential to the flame x (which is a result of the boundary layer assumption); and (4) the solution is considered along the x axis (stagnation stream plane) [11,13,14]. Thus, one can use the similarity solutions to reduce the governing equations to ordinary differential equations [11].

In the axisymmetric laminar diffusion flame, chemical reaction occurs in a relatively thin mixing layer formed in the vicinity of the stagnation plane. According to the analytical solution of counterflow diffusion flow under the assumption of Burke-Schumann [11], an estimate of mixing layer thickness δ_{mix} is $\sqrt{D/\chi}$, where D and χ are mass diffusion coefficient and scalar dissipation rate respectively. The mixing layer thickness is 0.1–0.2 cm. To simplify the problem, several approximations are introduced. Natural convection is neglected because the thickness of mixing layer (0.1–0.2 cm) is much smaller than the characteristic length (2 cm) above which buoyancy becomes dominant. Radiative heat loss is suppressed because flame conditions near the transport-induced extinction are considered [15]. Governing equations, boundary conditions with potential flow assumption, and the notation of variables can be found elsewhere [15,16]. Many researchers employed counterflow flame configuration to investigate diffusion flame combustion, and it was demonstrated valid [17–20].

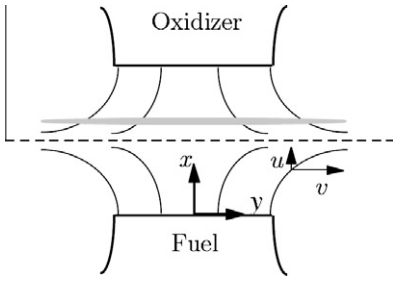

Fig. 1. Geometry of the opposed-flow diffusion flame. The dashed line represents the stagnation plane; the dotted region suggests the flame [11].

Using Cantera software code, counterflow diffusion flame of high-temperature off-gas of steelmaking converter is simulated. Cantera is an object-oriented [7,8], open source suite of software tools for reacting flow problems involving chemical kinetics, thermodynamics and transport processes. The adopted reaction scheme to describe combustion reactions in the flames is the GRI 3.0 mechanism that involves 53 species and 325 reactions [13,21]. The GRI 3.0 mechanism have been extensively validated in previous studies using a variety of configurations including perfectly stirred reactors, laminar flame speeds, and nonpremixed and partially premixed methane flames[22–24]. Therefore, the use of GRI 3.0 mechanism can used to model flames burning and NO_x emissions.

In counterflow diffusion flame, the global strain rate (α_g) allows quantification of a characteristic flame residence time or flow time, and it is defined as [23]

$$\alpha_g = \frac{2|V_O|}{L}\left(1+\frac{|V_F|\sqrt{\rho_F}}{|V_O|\sqrt{\rho_O}}\right) \quad (1)$$

where the V denotes the velocity, ρ denotes the density of the reactant streams at the duct boundaries, L is the duct separation distance, and the subscripts O and F represent the air and fuel streams, respectively. In the simulation described here, the global strain rate varies from 49 s^{-1} to 64 s^{-1}. Air stoichiometric ratio (SR) represents the fuel–air mixture composition

$$SR = (\text{actual air supplied})/(\text{stoichiometric air demand of fuel}) \quad (2)$$

In the simulation, off-gas of steelmaking converter consists of CO and CO_2; off-gas temperature at the fuel boundary varies from 1100 to 1900 K, air at the oxidizer boundary is kept at 300 K; air stoichiometric ratio varies from 0.6 to 1.4; the relative humidity (RH) in air supplied from 10% to 60%; CO concentration range is 10–60%; the separation distance (L) between fuel and oxidizer boundaries is 2 cm.

The relative axial distance (X) from fuel jet port is defined as

$$X = \frac{x}{L} \quad (3)$$

where the x denotes the axial distance from fuel jet port, and L is the duct separation distance, 2 cm.

Since no experimental data are available to validate the model of off-gas of steelmaking converter flames, we performed additional validation studies using the available measurements of the flame structure and NO_x profile in methane–air counterflow flame, and the experimental data refer to the reference [25]. Using the axisymmetric laminar diffusion flame model (see it in Fig. 1) and GRI 3.0 mechanism, the methane–air counterflow flame is simulated by Cantera software code. The burner system consists of two opposed cylindrical ducts, the distance between the two burners was maintained at 2 cm, fuel-rich $CH_4/O_2/N_2$ premixed reactant was injected through the bottom duct and air through the top (see Fig. 1), fuel stream equivalence ratio was 1.45, the global strain rate (α_g) was 20 s^{-1}, and the temperatures of fuel and air were 300 K. Fig. 2 presents a comparison of the measured and predicted the profiles of NO and temperature, there is an good agreement between the predicted and measured flame structures in terms of temperature and NO. However, the measured temperatures are 200–300 K higher than predictions in the flame zone. In the experiment [25], the thin filament pyrometry (TFP) technique used to measure temperatures, which involves extending a 10–20 μm diameter SiC fiber with weighted free ends across the centerline of the flame and measuring the radiant emission of the fiber using an infrared detector. This disagreement of the predicted and measured temperature might be explained [25] that the assumption of constant emissivity with wavelength and temperature may not hold for SiC fibers at the higher temperatures. In addition, not much is known about physical or chemical changes that might occur to the fiber material at temperatures approaching 2000 K. In GRI 3.0 mechanism, methane–air combustion deals with the reaction mechanisms of CO oxidization and NO_x formation, and thus the comparison of the measured and predicted the profiles of NO and temperature in methane–air combustion flame can validate the model of off-gas of steelmaking converter flame.

3. Results and discussion

3.1. Profile characteristics of temperature and major species in counterflow diffusion flame of off-gas

Fig. 3 shows a typical profiles of species mole fractions, species production rates and flame temperature of a off-gas counterflow diffusion flame (off-gas: CO = 40%, CO_2 = 60%, $T_{off\text{-}gas}$ = 1700 K; air: p = 1 atm, T_{air} = 300 K, RH = 30%) at SR = 1.05 and α_g = 49 s^{-1}. In Fig. 3, the dashed line shows the position of the stagnation plane, the maximum of temperature is located in off-gas side of the stagnation plane, and consequently the flame zone is formed at this location. According to the chemical stoichiometry, the mass of air required is less than that off-gas, the temperature of off-gas (1700 K) is much higher than that of air (300 K), and thus the flame occurs on off-gas side of the stagnation plane. In the region of flame, O_2 and CO concentrations and the production rates dramatically change. The location (X = 0.63), where CO and O_2 are nearly consumed coincides with that of the maximum temperature (T_{max} = 2003 K).

During fuel combustion, three principal NO_x forms are thermal NO_x, prompt NO_x, and fuel NO_x, and the relative contribution of each of the total NO_x formed depends on the combustion process and fuel characteristics. The importance of each of the three mechanisms varies, depending on combustion conditions including fuel,

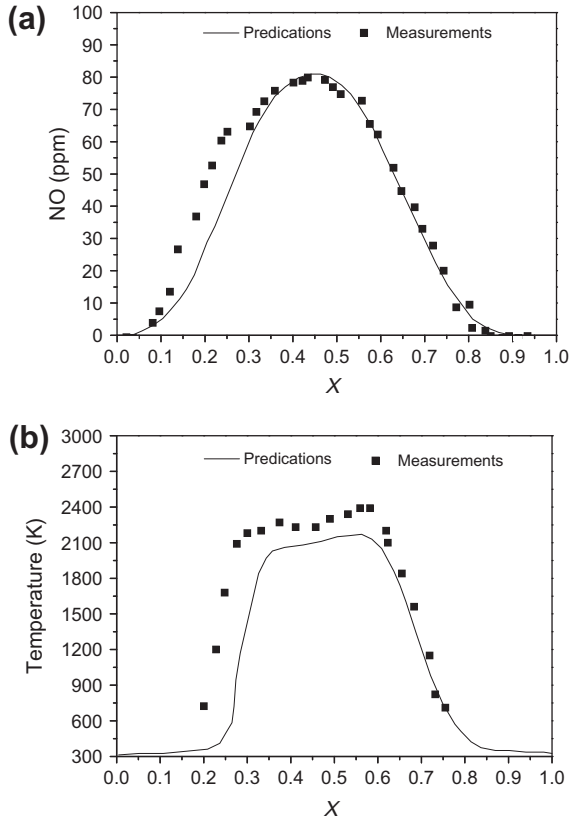

Fig. 2. Comparison of the predicted and measured NO mole fraction profiles flame temperature in methane–air counterflow flames at fuel stream equivalence ratio 1.45.

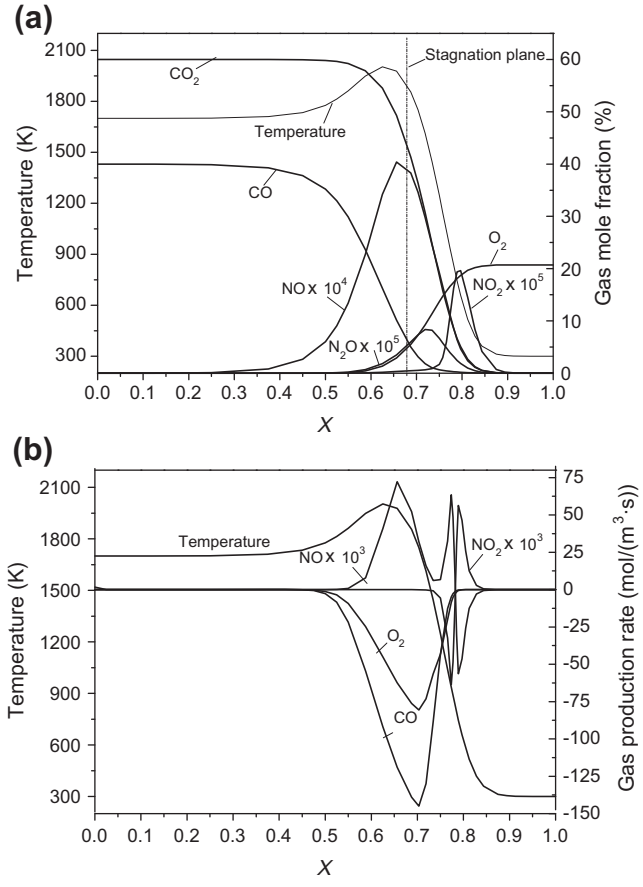

Fig. 3. Profiles of species mole fractions, species production rates and temperature.

combustion environment, and temperature. Since off-gas of steelmaking converter contains virtually no fuel nitrogen, the flame temperature reaches above 1800 K during high-temperature off-gas combustion, and the NO_x form is thermal NO_x. Thermal NO_x is formed from the reaction of nitrogen and oxygen supplied by the combustion air stream, and it is highly dependent on temperature and oxygen concentration. In Fig. 3, the location of the maximum NO (X = 0.66, T = 1986 K, NO = 40.4 ppm, and O_2 = 2.92%) is close to that of the maximum temperature (X = 0.63, T = 2003 K, NO = 36.2 ppm, and O_2 = 1.35%), and it demonstrates temperature sensitivity. Although thermal NO formation is highly dependent on temperature, O_2 concentration is very important to NO formation at high temperature, and the rate of formation of NO will increase with increasing oxygen concentration. Since the O_2 concentration at X = 0.66 is more twice than the O_2 concentration at X = 0.63, the maximum NO occurs at X = 0.66. In comparison to simulation result of Fig. 2, NO peak appears before maximum temperature in Fig. 2. For methane–air counterflow flame, the prompt-NO is important, it is most prevalent in rich flame, and thus NO peak appears before maximum temperature in Fig. 2.

In order to investigate NO_x reaction mechanisms, the reaction pathway flux analysis is performed using MixMaster (a Python program that is part of the Cantera suite) [7], and the integral path analysis is based on a conserved scalar approach to reaction fluxes. The analysis is visualized by a reaction path diagram, the diagram is a directed graph whose nodes are the chemical species, an edge connects two species if a reaction moves material from one to the other, the edge is drawn as an arrow from the reactant to the product, and the relative width of the arrows also provides an indication of pathway importance.

As known from Fig. 3a, the concentrations of NO, N_2O and NO_2 are respectively high at X = 0.63, 0.72 and 0.80, and thus formation mechanisms of nitrogen oxides at the three positions are investigated. Fig. 4 shows the NO_x reaction pathway diagrams at different axial position of the counterflow flame (see in Fig. 3).

Fig. 4a shows the nitrogen oxides reaction pathway diagram at X = 0.63, where flame temperature and NO mole fraction are maxima (T = 2003 K and NO = 36.2 ppm, see these in Fig. 3). The reaction pathway diagram indicates that NO is obtained by the following three mechanisms:

$$N_2 + O \rightarrow NO + N \quad (4)$$

$$N + O_2 \rightarrow NO + O \quad (5)$$

$$N + CO_2 \rightarrow NO + CO \quad (6)$$

$$N + OH \rightarrow NO + H \quad (7)$$

Reaction (4) is the first step of these reactions, it has a very high activation energy (E_a = 318 kJ/mol) due to the strong triple bond in the N_2-molecule, and is thus sufficiently fast only at high temperature. Because of its small reaction rate, reaction (4) is the rate-limiting step of the thermal NO-formation, and it is crucial for NO production [14].

Fig. 4b shows the nitrogen oxides reaction pathway diagram at X = 0.72, where N_2O mole fraction has its maximum (see it in

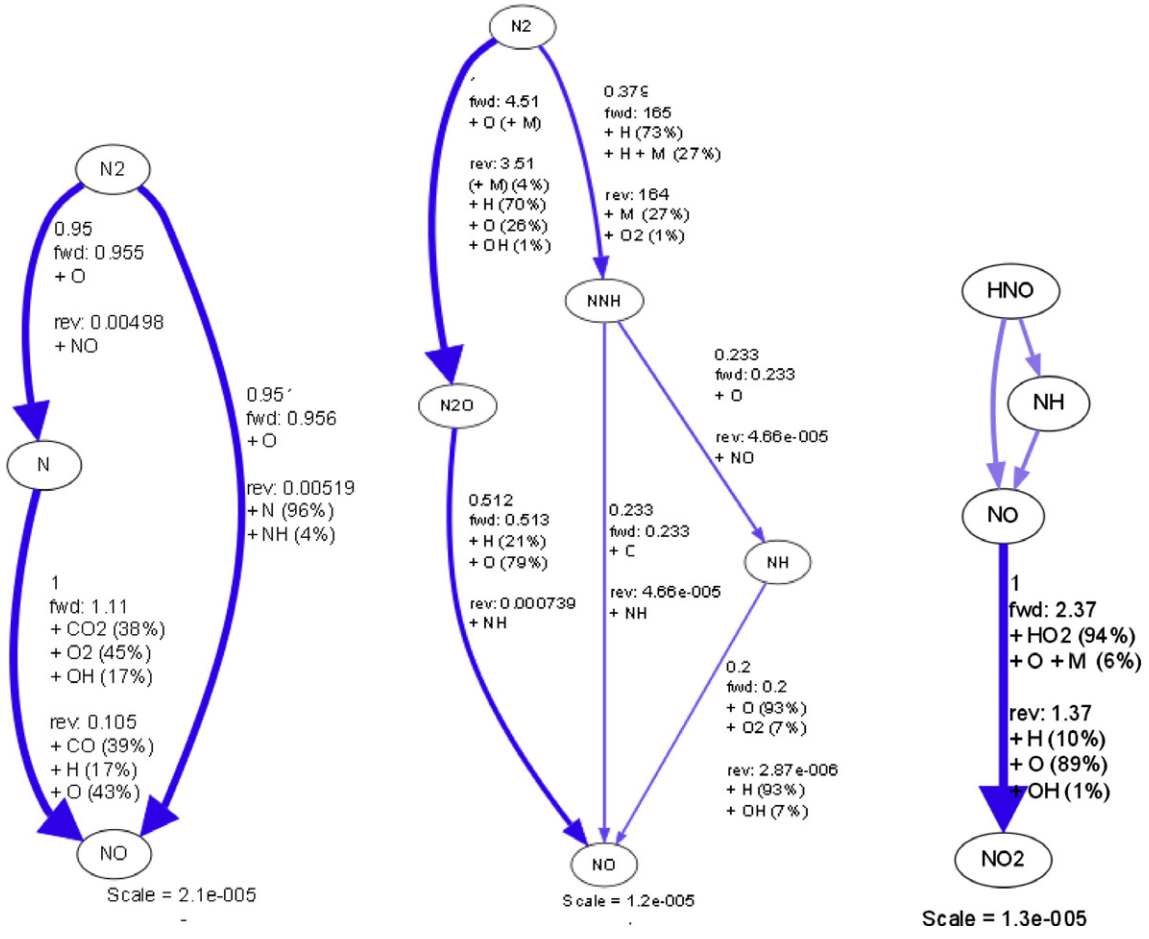

(a) X=0.63 (b) X=0.72 (c) X=0.80

Fig. 4. Nitrogen oxides reaction pathway diagrams.

Fig. 3). The reaction pathway diagram indicates that N_2O is mainly obtained by the following mechanism:

$$N_2 + O + M \rightarrow N_2O + M \quad (8)$$

N_2O mechanism is analogous to the reaction (4) mechanism in that O-atom attacks molecular nitrogen. However, with the presence of a third molecule M, the outcome of this reaction is N_2O. In Fig. 3, the local molar ratio of N_2O–NO is about 0.03, where N_2O mole fraction has its maximum, N_2O concentration is very low. The reaction has often been overlooked since it usually is an insignificant contributor to the total of NO [14]. The N_2O may subsequently react with O atoms to form NO

$$N_2O + O \rightarrow 2NO \quad (9)$$

Fig. 4c shows the nitrogen oxides reaction pathway diagram at $X = 0.80$, where NO_2 mole fraction has its maximum (see it in Fig. 3), and the local molar ratio of NO_2–NO_x is about 0.3. The reaction pathway diagram indicates that NO_2 is mainly obtained by the following mechanism:

$$NO + HO_2 \rightarrow NO_2 + OH \quad (10)$$

NO_2 formation from NO tends to occur in the region, where rapid cooling takes place, such as the mixing region of hot combustion gases with the inlet air, the amount of NO_2 formed increases with increasing cooling rate of the combustion gas, and the NO_2/NO ratio increase with decreasing initial NO concentration [25].

Fig. 5 shows the reaction pathway diagrams of CO oxidation and OH formation at $X = 0.63$, where flame temperature is maximum ($T = 2003$ K, see it in Fig. 3). The reaction pathway diagram indicates that CO oxidation is mainly obtained by the following mechanism:

$$CO + OH \rightarrow CO_2 + H \quad (11)$$

Therefore, OH is very crucial to CO oxidation. It is difficult to ignite and sustain a dry CO–O_2 flame because the direct reaction between CO and O_2,

$$CO + O_2 \rightarrow CO_2 + O \quad (12)$$

has a high activation energy (200.64 kJ/mol) and therefore is very slow process even at high temperature. Furthermore, the O-atom produced does not lead to any rapid chain-branching reactions. However, in the presence of even a small quantity of hydrogen-containing material, OH radicals are formed to accelerate the CO oxidation [26,27]. For off-gas of steelmaking converter combustion, off-gas contains virtually no hydrogen-containing material, OH only originates from H_2O vapor in combustion air stream supplied. As known from Fig. 5b, OH is principally obtained by the following mechanisms:

$$H_2O + O \rightarrow 2OH \quad (13)$$

$$H_2O + H \rightarrow OH + H_2 \quad (14)$$

Therefore, during off-gas of steelmaking converter combustion, H_2O vapor in air supplied is important, and the absence of H_2O may make the oxidation of CO extremely slow.

3.2. Characteristics of NO_x emissions

During off-gas of steelmaking converter combustion, nitrogen oxides depend principally on the temperature and stoichiometric ratio in combustion zone. In the section, the influences of CO concentration, off-gas temperature and stoichiometric ratio on NO_x emissions are investigated.

NO_2 is formed from NO on the lean side of the flame (see Fig. 3), and it is a significant emission. Since the NO_2 is formed through NO, its formation does not alter the total pollutant emissions, NO_x emissions are reported in terms of the sum of NO_2 and NO emissions.

The characteristics of NO_x emissions can be represented by the emission index of NO_x ($EINO_x$), it describes the grams of NO_x produced per kilogram of fuel consumed after all NO_x has been converted by convention to NO_2, and here this is found

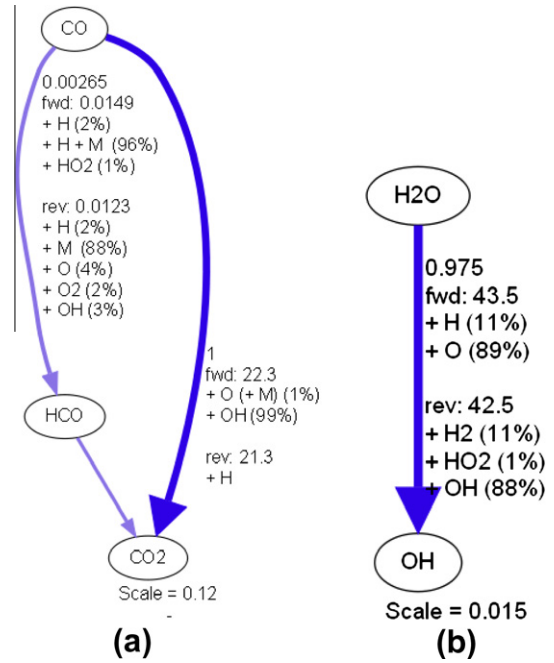

Fig. 5. CO oxidation and OH reaction pathway diagrams at $X = 0.66$ ($T = 1978$ K).

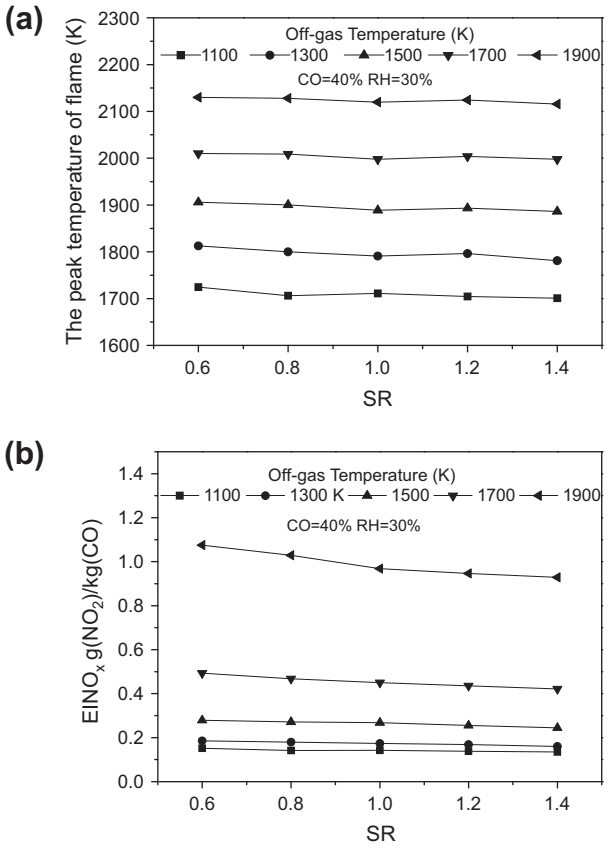

Fig. 6. The influence of SR on $EINO_x$ at different off-gas temperature.

computationally by integrating the reaction rates across the flame as

$$\mathrm{EINO}_x = \frac{1000 \times \mathrm{W}_{\mathrm{NO}_2} \int_0^L (w_{\mathrm{NO}} + w_{\mathrm{NO}_2}) dx}{-\mathrm{W}_{\mathrm{CO}} \int_0^L w_{\mathrm{CO}}\, dx} \quad (15)$$

where W_i and w_i are, respectively, the molecular weight and molar production rate of species i, and L is the separation distance between off-gas and air boundaries.

Fig. 6 shows influence of stoichiometric ratio and off-gas temperature on EINO_x at 40% CO and 30% RH. Increasing air stoichiometric ratio makes the peak temperature of flame and EINO_x marginally decrease. Although increasing air stoichiometric ratio is conducive to off-gas combustion, the combustion heat value of off-gas is low because of low CO concentration in off-gas, and the combustion heat cannot totally offset the absorption heat of cool air supplied. Therefore, increasing air stoichiometric ratio makes the flame temperature marginally decrease, and then EINO_x marginally decreases, as shown in Fig. 6b.

As known from Fig. 6, with the increase of off-gas temperature at a given SR, the peak temperature of flame stably increases, and EINO_x dramatically increases when the off-gas temperature is over 1500 K (see Fig. 6b). For high-temperature off-gas of steelmaking converter combustion, increasing off-gas temperature results in the increase of the off-gas flame temperature. During off-gas of steelmaking converter combustion, NO_x is thermal NO_x. Based on chemical reaction kinetics, thermal NO_x is very temperature sensitive and is produced vastly at combustion temperature of approximately 1900–2200 K [28]. As known from Fig. 6a, the peak temperature of combustion flame reaches over 1900 K when off-gas of steelmaking converter temperature is greater than 1500 K, and thus a large amount of thermal NO_x is formed, which makes EINO_x dramatically increase with the temperature of off-gas of steelmaking converter (see Fig. 6b).

Fig. 7 shows the influence of CO concentration on NO_x emissions and the peak temperature of flame at different off-gas temperature. With the increase of CO concentration, the rising trend of the peak NO_x concentration is similar to that of EINO_x. The heat value of off-gas of steelmaking converter increases with CO concentration, and then increasing CO concentration of off-gas makes combustion flame temperature increase, which results in the increase of thermal NO_x formation. When off-gas temperature is 1700 K, the peak temperature is over 1900 K, and thus NO_x levels increase dramatically with CO concentration [28].

3.3. Characteristics of CO burnout

During off-gas of steelmaking converter combustion in cooling stack, CO is often over-standard emission. In the section, some influencing factors of CO burnout are investigated. In order to describe CO burnout in counterflow diffusion flame, CO burnout index ($\mathrm{BI}_{\mathrm{CO}}$) is defined as

$$\mathrm{BI}_{\mathrm{CO}} = \frac{-\mathrm{W}_{\mathrm{CO}} \int_0^L w_{\mathrm{CO}}\, dx}{\mathrm{m}_{\mathrm{CO}}} \quad (16)$$

where W_{CO} and w_{co} are, respectively, the molecular weight and molar consumption rate of CO, L is the separation distance between fuel and oxidizer boundaries, and m_{co} is the mass flowrate of CO at fuel inlet. High $\mathrm{BI}_{\mathrm{CO}}$ means high CO combustion burnout.

Fig. 8 shows the influence of off-gas temperature, SR and CO concentration on CO burnout. Fig. 8a indicates that increasing off-gas temperature and stoichiometric ratio makes $\mathrm{BI}_{\mathrm{CO}}$ increase

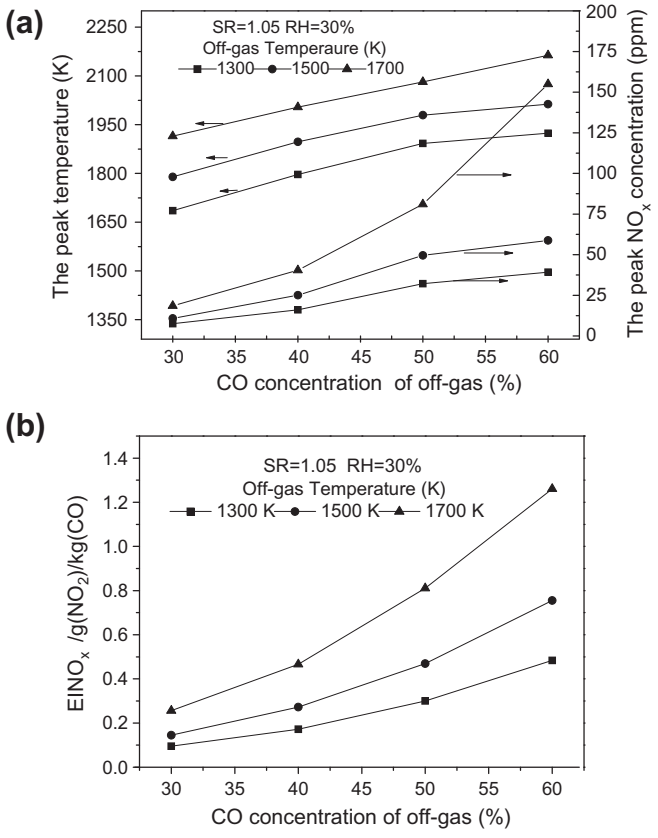

Fig. 7. The influence of CO concentration on NO_x emissions and the peak temperature of flame at different off-gas temperature.

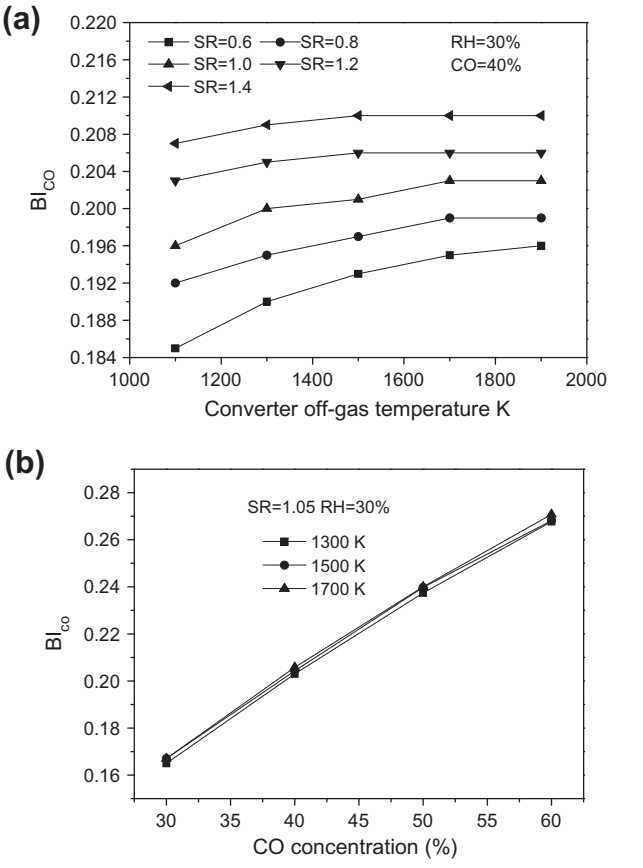

Fig. 8. The influence of off-gas temperature, SR and CO concentration on CO burnout.

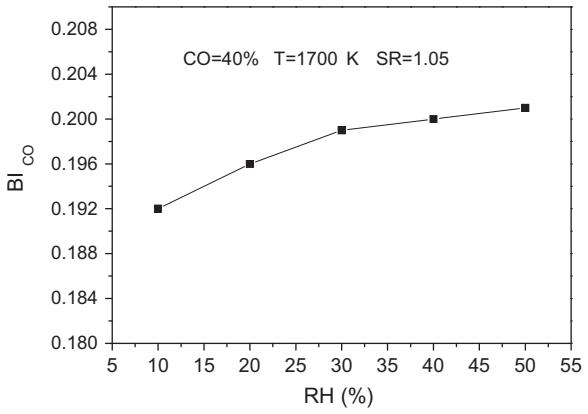

Fig. 9. The influence of the relative humidity in air supplied on CO burnout.

at SR ⩽ 1.0. For fuel-rich combustion flame (SR ⩽ 1.0), increasing air stoichiometric ratio makes O_2 easily diffuse into off-gas to oxidize CO in counterflow diffusion flame. In the meantime, increasing off-gas temperature makes flame temperature increase (see Fig. 7a), the forward reaction rate of the main CO oxidation reaction mechanism (11) increases. Therefore, for fuel-rich combustion flame (SR ⩽ 1.0), increase off-gas temperature or/and stoichiometric ratio makes BI_{CO} increases notably (see Fig. 8a). For high-temperature fuel-lean combustion flame (SR > 1.0) at a given SR, combustion temperature is not main combustion controlling factor, and thus the influence of off-gas temperature on BI_{CO} is marginal (see Fig. 8a).

Fig. 8b shows the influence of CO concentration in off-gas on CO burnout at different off-gas temperature, and it indicates that: the increase of CO concentration in off-gas makes BI_{CO} increase, and the influence of off-gas temperature on CO burnout index is marginal. Since off-gas of steelmaking converter consists of CO and CO_2, high CO_2 dilutes CO in combustion flame, which is not conducive to CO diffusion combustion. Increasing CO concentration in off-gas is conducive to increase BI_{CO}.

Fig. 9 shows the influence of the relative humidity in air supplied on CO burnout index. BI_{CO} increases with the relative humidity in air supplied. As known from Fig. 5, CO oxidation is mainly obtained by reaction mechanism (11), OH is very crucial to CO oxidation. For off-gas of steelmaking converter combustion, OH only originates from H_2O vapor in air supplied. Therefore, during off-gas of steelmaking converter combustion, air supplied with high relative humidity can provide more H_2O vapor to form OH radicals in combustion flame, OH radicals formed can accelerate the CO oxidation, and thus BI_{CO} increases with the relative humidity in air supplied. During CO oxidation reaction, OH radicals formed are recirculated and not really consumed, a small quantity of hydrogen-containing material is enough to accelerate the CO oxidation, and thus BI_{CO} marginally increases at RH ⩾ 30% (see Fig. 9).

4. Conclusions

During off-gas of steelmaking converter combustion in cooling stack, CO and NO_x are often over-standard discharge. High-temperature off-gas combustion is simulated by adopting counterflow diffusion flame as a model. During counterflow diffusion combustion of off-gas, NO_x emissions index marginally decreases with air stoichiometric ratio (SR), and it dramatically increases with off-gas temperature at a given SR when the off-gas temperature is over 1500 K. High CO concentration in off-gas can results in high $EINO_x$, and NO_x levels increase dramatically with CO concentration when off-gas temperature is over 1700 K. Both air stoichiometric ratio and off-gas temperature are important for CO burnout at SR ⩽ 1.0, but the influence of off-gas temperature on CO burnout is marginal at SR > 1.0. CO burnout index increases notably with CO concentration in off-gas, but the influence of off-gas temperature on CO burnout index is marginal. CO burnout index increases with the relative humidity in air supplied, but it marginally increases at RH ⩾ 30%.

Acknowledgement

Financial supports by National Natural Science Foundation of China (Nos. 50976123, 50976122) is acknowledged.

References

[1] Aleksashin AL, Schnaltzger I, Hollias G. Creation and growth of oxygen-converter steelmaking. Metallurgist 2007;51:60–5.
[2] Li S. Study on the formation, flow, and reaction process of metallurgical furnace off-gas/flue gas. Chinese Academy of Sciences Post-Doctoral Work Report; 2010.
[3] Engelmann A, Huber R, Unger K. Dynamic simulation of cooling stack and cooling circuit for converter gas cooling. Ironmak Steelmak 2007;34:54–60.
[4] Bada H, Yamada S, Yaji M, Kodaka SFM. Improvement in off-gas recovery from Q-BOP. Kwasaki Steel Technical Report; 1983.
[5] Emission standards for iron and steel industry (DB37/990-2008). <http://www.sdein.gov.cn/art/2008/5/15/art_39_128545.html>.
[6] Li S, Xu TM, Sun P, Zhou QL, Tan HZ, Hui SE. NO_x and SO_x emissions of a high sulfur self-retention coal during air staged combustion. Fuel 2008;87:723–31.
[7] Object-oriented software for reacting flows. <http://www.cantera.org>.
[8] Law CK. Combustion at a crossroads: status and prospects. Proc Combust Inst 2007;31:1–29.
[9] Toro VV, Mokhov AV, Levinsky HB, Smookec MD. Combined experimental and computational study of laminar, axisymmetric hydrogen–air diffusion flames. Proc Combust Inst 2005;30:485–92.
[10] Cho ES, Chung SH. Numerical evaluation of NO_x mechanisms in methane–air counterflow premixed flames. J Mech Sci Technol 2009;23:659–66.
[11] Lutz AE, Kee RJ, Grcar JF. OPPDIF: a fortran program for computing opposed-flow diffusion flames Sandia national laboratories. Report no. SAND96-8243, 1996.
[12] Nickel K. Prandtl's boundary-layer theory from the viewpoint of a mathematician. Ann Rev Fluid Mech 1973;5:405–28.
[13] Schlichting H, Gersten K. Boundary layer theory. 8th Revised and enlarged edition. New York: Springer-Verlag; 2000.
[14] Warnatz J, Maas U, Dibble RW. Combustion: physical and chemical fundamentals, modeling and simulation, experiments, pollutant formation. Springer; 2006.
[15] Sohn CH, Kim JS, Chung SH, Maruta K. Nonlinear evolution of diffusion flame oscillations triggered by radiative heat loss. Combust Flame 2000;123:95–106.
[16] Giovangigli V, Smooke MD. Extinction of strained laminar flames with complex chemistry, combust. Sci Technol 1987;53:23–49.
[17] Li SC, Williams FA. Counterflow heptane flame structure. Proc Combust Inst 2000;28:1031–8.
[18] Toro VV. Experimental study of the structure of laminar axisymmetric H_2/air diffusion flames. PH.D dissertation 2006. University of Groningenm. <http://irs.ub.rug.nl/ppn/297262513>.
[19] Som S, Ramírez AI, Hagerdorn J, Saveliev A, Aggarwal SK. A numerical and experimental study of counterflow syngas flames at different pressures. Fuel 2006;85:1729–42.
[20] Drake MC, Blint RJ. Thermal NO_x in stretched laminar opposed-flow diffusion flames with CO/H_2/N_2 fuel. Combust Flame 1989;76:151–67.
[21] Smith GP, Golden DM, Frenklach M, Moriarty NW, Eiteneer B, Goldenberg M, et al. GRI-3.0. <http://www.me.berkeley.edu/grimech/>.
[22] Som S, Ramírez AI, Hagerdorn J, Saveliev A, Aggarwal SK. A numerical and experimental study of counterflow syngas flames at different pressures. Fuel 2008;87:319–34.
[23] Giles DE, Som S, Aggarwal SK. NO_x emission characteristics of counterflow syngas diffusion flames with airstream dilution. Fuel 2006;85:1729–42.
[24] Kim JS, Park J, Bae DS, Vu TM, Ha JS, Kim TK. A study on methane–air premixed flames interacting with syngas–air premixed flames. Int J Hydrogen Energy 2010;35:1390–400.
[25] Ravikrishna RV, Laurendeau NM. Laser-induced fluorescence measurements and modeling of nitric oxide in counterflow partially premixed flames. Combust Flame 2000;122:474–82.
[26] Morio H. Experimental study of nitrogen dioxide formation in combustion systems. Symposium (Int) Combust 1988; 21:1181–88.
[27] Law CK. Combustion physics. Cambridge University Press; 2006.
[28] Annamalai K, Puri IK. Combustion science and engineering. CRC Press; 2006.